

## New Mechanistic Insight in the Thermal Helix Inversion of Second-Generation Molecular Motors

Martin Klok, Martin Walko, Edzard M. Geertsema, Nopporn Ruangsupapichat, Jos C. M. Kistemaker, Auke Meetsma, and Ben L. Feringa\*<sup>[a]</sup>

**Abstract:** The introduction of dibenzocyclohepten-5-ylidene as part of a unidirectional light-driven molecular motor allows a more complete picture of the pathway of thermal helix inversion to be developed. The most stable conformation is similar to that found in related motors in that it has, overall, an *anti*-folded structure with the substituent at the stereogenic centre adopting an axial orientation. Photochemical *cis/trans* isomerisation at  $-40^{\circ}\text{C}$  results in the formation of an isomer in a *syn*-folded conformation with the methyl group in an axial orientation. This contrasts with previous studies on related

molecular rotary motors. The conformation of the higher energy intermediate typically observed for this class of compound is the *anti*-folded conformation, in which the methyl group is in an equatorial orientation. This conformation is available through an energetically uphill upper half ring inversion of the observed photochemical product. However, this pathway competes with a second process that leads to the more

stable *anti*-folded conformation in which the methyl group is oriented axially. It has been shown that the conformations and pathways available for second-generation molecular motors can be described by using similar overall geometries. Differences in the metastable high-energy species are attributable to the relative energy and position on the reaction coordinate of the transition states. Kinetic studies on these new molecular motors thus provide important insights into the conformational dynamics of the rotation cycle.

**Keywords:** alkenes • conformational dynamics • helical structures • molecular motors • nanotechnology

### Introduction

The design of artificial molecular motors is of major importance for the development of nanomachines and dynamic systems and devices. Natural systems, for example, ATPase<sup>[1]</sup> and kinase,<sup>[2]</sup> which perform complex machine-like tasks routinely, have inspired scientists to pursue the development of systems that provide dynamic functionality at the molecular level.<sup>[3]</sup> Powering such devices requires motors that convert one form of energy into another. To this end, several approaches have been explored,<sup>[4]</sup> including linear shuttles,<sup>[5]</sup>

muscles<sup>[6]</sup> and rotary systems.<sup>[7]</sup> Repetitive unidirectional rotary motion has been achieved in only a few cases.<sup>[8]</sup> In our first unidirectional rotary motor two identical chiral moieties were connected to a central double bond, which functioned as the axis of rotation.<sup>[9]</sup> The second-generation motors, which function by the same principle, use a symmetric lower half stator unit, allowing for more possibilities in terms of functionalisation. In this case a rotor is connected through an alkene, which functions as the axis of rotation, to a stator unit (Figure 1).<sup>[10]</sup>

The dynamic folding and conformational interconversion during rotation of second-generation systems has been established for a series of molecular motors, in which X and Y are different atoms or groups (Figure 2). Structural studies by X-ray crystallographic analysis, <sup>1</sup>H NMR spectroscopy and molecular modelling on several systems (X = CH<sub>2</sub> or S; Y = S, C(CH<sub>3</sub>)<sub>2</sub> or – Figure 2) have shown that in the most stable conformation the molecules adopt a helical shape with a methyl group in a pseudo-axial orientation. The helicity is dictated by the absolute configuration at the stereogenic centre, that is, the methyl group. These molecules adopt an overall *anti*-folded conformation around the cen-

[a] Drs. M. Klok, M. Walko, Dr. E. M. Geertsema, N. Ruangsupapichat, J. C. M. Kistemaker, Dr. A. Meetsma, Prof. Dr. B. L. Feringa  
Laboratory of Organic Chemistry  
Stratingh Institute for Chemistry  
and Zernike Institute for Advanced Materials  
Faculty of Mathematics and Natural Sciences  
University of Groningen, Nijenborgh 4  
9747 AG, Groningen (Netherlands)  
Fax: (+31)50-363-4278  
E-mail: b.l.feringa@rug.nl

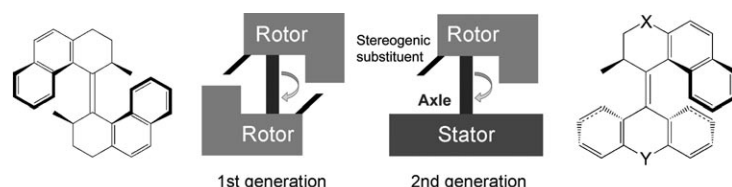


Figure 1. First- (left) and second-generation (right) molecular motors.

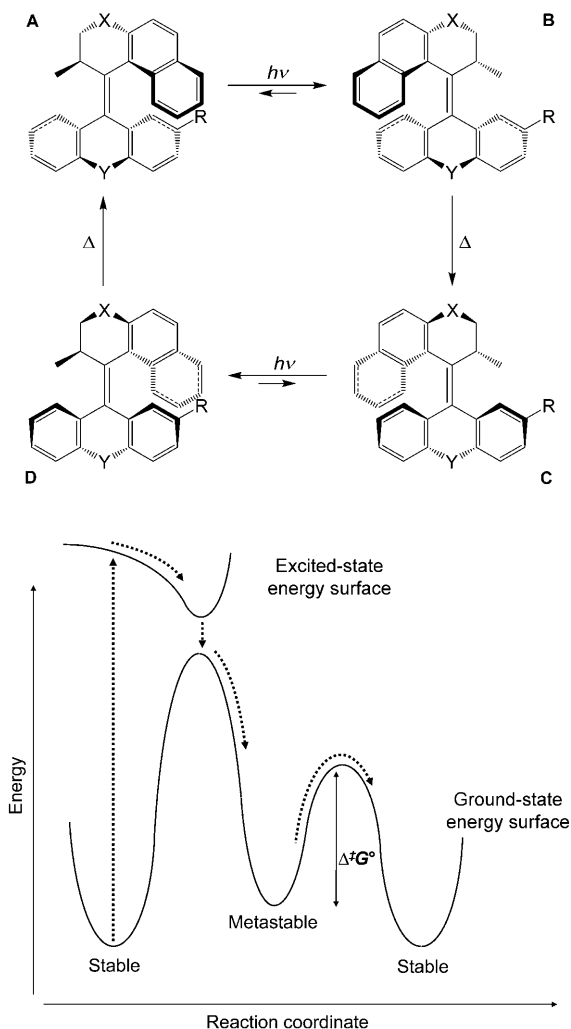


Figure 2. Rotation mechanism (top) and energy profile (bottom) for second-generation molecular motors.

tral double bond, with the X and Y groups pointing in opposite directions (Figure 2, **A** and **C**).<sup>[10]</sup> For the case in which the lower half is a fluorenyl moiety ( $Y = \text{CH}_2, -$ ), this geometry is better described as planar-folded because of the absence of a folded conformation in the fluorene moiety.<sup>[11]</sup> Higher energy, thermally unstable isomers **B** and **D** (Figure 2) are different in that the methyl group at the stereogenic centre is positioned in a more sterically hindered pseudo-equatorial orientation. The overall geometry remains helical, but with opposite helicity to that of the stable form. However, an *anti*-folded geometry is encountered in

every case investigated. The following describes the mechanism for rotation (Figure 2): A photochemical *cis/trans* isomerisation of stable form **A** results in the formation of a second isomer **B**, which has a higher energy due to the more hindered pseudo-equatorial orientation of the methyl group at

the stereogenic centre. The overall helicity of the molecule is inverted in this process, although the conformation around the central double bond is still *anti*-folded. Fluorenyl stator units are an exception to this because of the absence of low-energy conformational folding due to the rigidity of the planar fluorene. This results in a twisted conformation for the higher energy conformer for such systems. However, in this structure the substituent at the stereogenic centre adopts the same pseudo-equatorial orientation. In all cases conformational relaxation occurs through a thermally activated helix inversion, in which the equatorial  $\rightarrow$  axial transition of the methyl substituent is accompanied by the naphthalene part passing over the lower half, thus restoring the original stable geometry (Figure 2, **C**). A repetition of these steps by the photochemical conversion of **C** to **D** results in a higher energy conformer with opposite helicity. This is followed by a second thermally activated helix inversion, converting **D** to the original conformation **A** and completing one  $360^\circ$  rotation. The direction of rotation is dictated by the absolute configuration at the stereogenic centre and the unidirectionality of the thermal helix-inversion step is the result of the lower energy associated with axial orientation. During the full rotation cycle, no other conformational isomers have been detected for second-generation motors, even in cases in which high thermal barriers are involved. However, stepwise helix inversion has been observed in a first-generation system.<sup>[12]</sup>

These conformational changes are related to those observed in conformational studies performed on structurally related bistricyclic aromatic overcrowded alkenes (Figure 3).<sup>[13]</sup>

For bithioxanthylene, the *anti*-folded conformer was found to be lowest in energy. The *syn*-folded conformer is  $14 \text{ kJ mol}^{-1}$  higher in energy and is not present in significant amounts in the thermal equilibrium.<sup>[13b]</sup> The twisted confor-

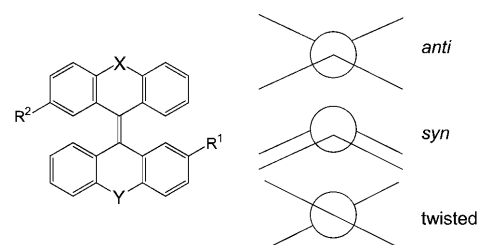
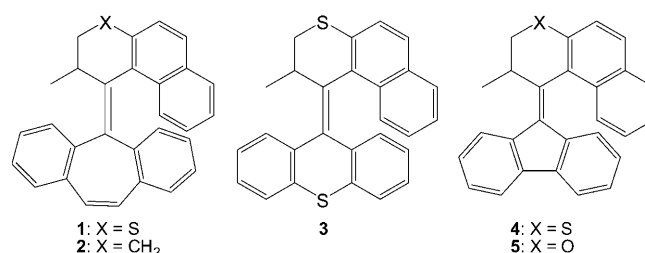


Figure 3. General structure (left) and conformations (right) of bistricyclic overcrowded alkenes (a more detailed overview of all possible conformations can be found in ref. [13]).

mation corresponds to a thermally unstable saddle point for these structures. In contrast, for overcrowded di-5*H*-dibenzocyclohepten-5-ylidene, the most stable conformation is the *anti*-conformer with the *syn* conformer being only 2.1 kJ mol<sup>-1</sup> higher in energy.<sup>[13,14]</sup> Both species can be observed in solution and thermal interconversion between these two conformers proceeds readily at room temperature. From these observations, it is evident that bis-5*H*-dibenzocyclohepten-5-ylidene constitutes an exception amongst the ditricyclic (bistricyclic for identical substituents) overcrowded alkenes because it is the only example to have a stable *syn*-folded conformation. In addition, it has been shown that upon photochemical *cis/trans* isomerisation the *anti* conformation is converted to the *syn* conformation.<sup>[13,14]</sup> On this basis it must be considered likely that the dibenzocyclohepten-5-ylidene overcrowded alkene motor (**1**) could display comparable conformational behaviour.

The fact that *syn*-folded conformers have not been encountered in second-generation molecular motors can be attributed to the asymmetric profile of steric hindrance in comparison with that in bistricyclic aromatic overcrowded alkenes. On one side of the double bond, second-generation molecular motors comprise a naphthalene unit rather than a phenyl unit, with a concomitant increase in steric hindrance. On the other side of the double bond, the replacement of a phenyl group with a (much smaller) methyl-substituted stereogenic centre introduces an extra degree of freedom. The possibility for this group to adopt either an equatorial or an axial orientation gives rise to the second, higher energy conformer, because a methyl group in an axial orientation experiences less steric hindrance with the stator part than a methyl group in an equatorial orientation. A twisted conformation is suspected to be involved in the thermal pathway to the lowest energy conformation, based on observations for bistricyclic aromatic overcrowded alkenes.<sup>[13]</sup> Thermally stable, twisted conformations have been characterised for bisfluorenylidene,<sup>[15]</sup> and likewise for fluorenylidene motors.<sup>[11]</sup> Moreover, in studies on the racemisation barriers of symmetric bistricyclic aromatic overcrowded alkenes, it was found that the aryl–X bond length affects the rates of racemisation and isomerisation considerably.<sup>[16]</sup> This was rationalised by an increase in steric hindrance in the fjord region with longer aryl–X bonds. A combination of conformational flexibility and steric repulsion, which can be, to some extent, governed by the aryl–X and aryl–Y bond lengths, is therefore expected to be important in determining the mechanism and rate of motor rotation.

Introducing molecular motors into functional devices requires detailed insight into the mechanism of rotation. For this reason we present a study of the thermal helix-inversion step in the mechanism of rotation of second-generation, light-powered, unidirectional molecular motors (Scheme 1), and additional insights obtained from one specific example of an exceptional mechanism of rotation.



Scheme 1. Molecular motors **1–5** described in this study.

## Results and Discussion

Irradiation of stable **1a** with 312 nm light at –40 °C overnight resulted in a single higher energy isomer, denoted **1b** (photostationary state stable **1a**/unstable **1b** = 58:42). In contrast, irradiation with 312 nm light overnight at 20 °C resulted in the formation of an additional isomer, denoted **1c** (ratio of stable **1a**/unstable **1b**/unstable **1c** = 58:25:18). Both new isomers represent higher energy conformations of **1a**, which is confirmed by the full conversion of the mixture of **1a/1b/1c** to **1a** upon heating (60 °C, 1 h). The small coupling constants of the stereogenic proton with the neighbouring protons <sup>3</sup>*J*(H<sup>A</sup>,H<sup>B</sup>) and <sup>3</sup>*J*(H<sup>A</sup>,H<sup>C</sup>) in isomer **1b** (*J* = 7.7 and 5.9 Hz; Table 1) reveal that this isomer has its methyl sub-

Table 1. Chemical shifts, coupling constants of the proton at the stereogenic position (H<sup>A</sup>) with neighbouring ring protons H<sup>B</sup> and H<sup>C</sup>, and the overall geometry for all stable isomers of **1** in [D<sub>8</sub>]toluene.

|                    | δ [ppm]                             | <sup>3</sup> <i>J</i> (H <sup>A</sup> ,H <sup>B</sup> ) and <sup>3</sup> <i>J</i> (H <sup>A</sup> ,H <sup>C</sup> ) [Hz] | δ [ppm]                 | Geometry    |
|--------------------|-------------------------------------|--|-------------------------|-------------|
| stable <b>1a</b>   | H <sup>A</sup> <sub>eq</sub> , 3.69 | 8.2, 5.1   | Me <sub>ax</sub> , 0.52 | <i>anti</i> |
| unstable <b>1b</b> | H <sup>A</sup> <sub>eq</sub> , 3.10 | 7.7, 5.9   | Me <sub>ax</sub> , 0.77 | <i>syn</i>  |
| unstable <b>1c</b> | H <sup>A</sup> <sub>ax</sub> , 2.20 | 11.9, 7.0  | Me <sub>eq</sub> , 0.58 | <i>anti</i> |

stituent in an axial orientation and is comparable to the most stable conformation **1a** (*J* = 8.2 and 5.1 Hz). On the other hand, the higher values for the same coupling constants in isomer **1c** (*J* = 11.9 and 7.0 Hz) indicate that here the methyl group adopts an equatorial orientation.

Kinetic studies were performed on sample mixtures in [D<sub>8</sub>]toluene irradiated at –40 °C for 5 h. Subsequently, <sup>1</sup>H NMR spectra were recorded at a fixed temperature every 2 min. It was found that conversion to the second unstable isomer, **1c**, does not go to completion, but rather **1c** is in equilibrium with the first unstable isomer, **1b**. The **1c** ⇌ **1b** equilibrium is reached more rapidly than conversion to stable form **1a**. At temperatures below 20 °C the conversion to **1a** is less than 2% by the time **1b** and **1c** reach equilibrium (*t* = 8000 s, Figure 4B). Eyring analysis in the range of –5 to +10 °C provided the activation parameters for the

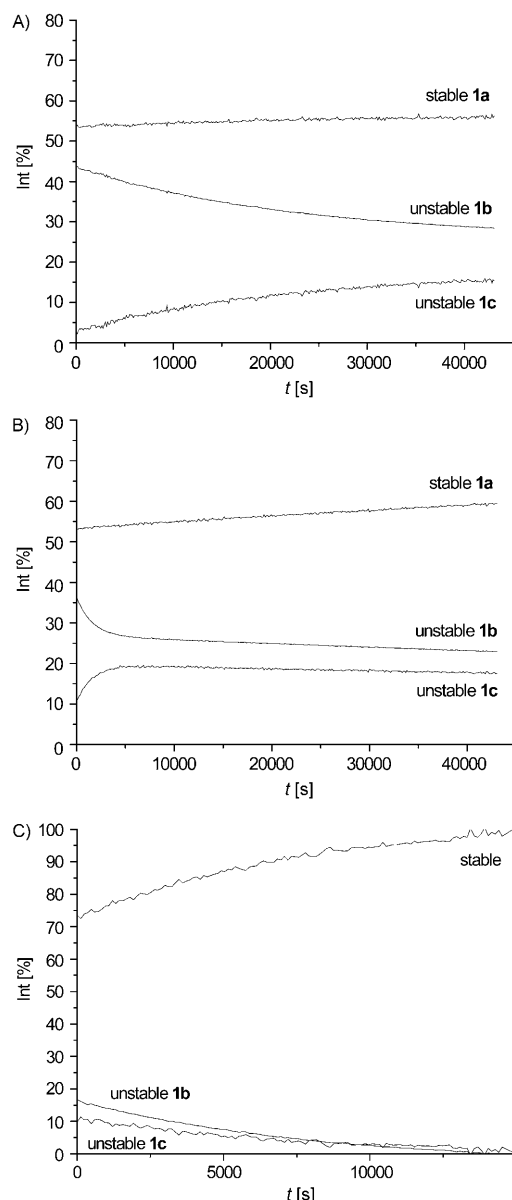


Figure 4. Conversion of structures **1a**⇌**1c** at 0 (A), 20 (B) and 50 °C (C) as determined by <sup>1</sup>H NMR in [D<sub>8</sub>]toluene.

**1b**⇌**1c** equilibrium. We found the barrier of activation for the conversion of unstable **1b** to unstable **1c** is 93.0 kJ mol<sup>-1</sup>, whereas the barrier of activation for conversion of unstable **1c** to unstable **1b** is 91.8 kJ mol<sup>-1</sup> (Table 2). By analysis of the rate of formation of **1a** in the temperature range from 30 to 60 °C under **1b**⇌**1c** equilibrium conditions, we determined the barrier of activation for this pro-

Table 2. Activation parameters for thermally activated transitions for compound **1**.

|                       | $\Delta^\ddagger G^\circ$ [kJ mol <sup>-1</sup> ] | $\Delta^\ddagger H^\circ$ [kJ mol <sup>-1</sup> ] | $\Delta^\ddagger S^\circ$ [JK <sup>-1</sup> mol <sup>-1</sup> ] |
|-----------------------|---|---|---|
| <b>1b</b> → <b>1a</b> | 101.5   | 85.4  | -57.4   |
| <b>1b</b> → <b>1c</b> | 93.0  | 68.9  | -82.1   |
| <b>1c</b> → <b>1b</b> | 91.8  | 71.1  | -70.7   |

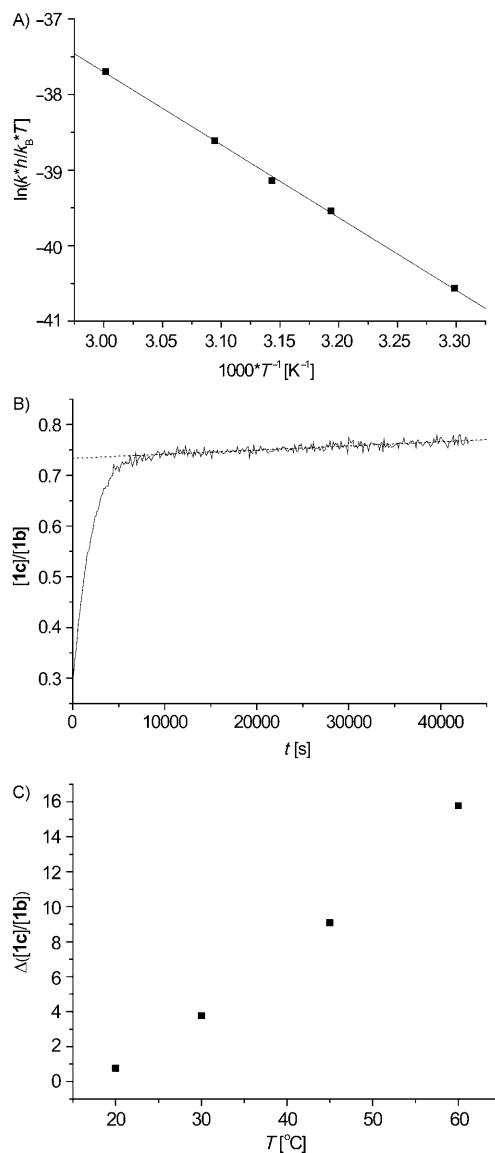


Figure 5. A) Eyring plot for the conversion of unstable **1b** to stable **1a** in [D<sub>8</sub>]toluene. B) Relative increase in [**1c**] relative to [**1b**] in time at 20 °C. C) Increase in [**1c**]/[**1b**] over time versus temperature under **1b**⇌**1c** equilibrium conditions.

cess to be 101.5 kJ mol<sup>-1</sup> (Figure 5A). Unimolecular behaviour was observed for all processes.

Conversion to stable **1a** is accompanied by a relative increase in unstable **1c**. At higher temperatures, at which **1b** and **1c** rapidly equilibrate, the increase in unstable **1c** relative to unstable **1b** occurs faster, as does the conversion to stable **1a**. This can be seen clearly by the slope of the [**1c**]/[**1b**] quotient over time (Figure 5B). After an initial equilibration period during which the relative amount of **1c** increases sharply, the ratio of **1c** relative to **1b** keeps rising. This is apparent from the slope of the linear part of the curve in the right-hand part of Figure 5B. At higher temperature, the slope of this line increases, reflecting the faster conversion to stable **1a** (Figure 5C). At 20 °C slow **1b**⇌**1c** equilibration ( $t=0$ –8000 s) is observed and thereafter **1b**

and **1c** remain at equilibrium ( $t > 8000$  s, Figure 4B), as the sample reverts to **a**. The observed rate of appearance of **1a** is higher under non-equilibrium conditions, at which the concentration of **1b** is much higher than that of **1c**. Under equilibrium conditions at  $t > 8000$  s, the rate of recovery of **1a** is  $3.2 \times 10^{-6} \text{ s}^{-1}$ , whereas the average rate of recovery of **1a** in the time range 0–480 s is approximately three times higher at  $9.2 \times 10^{-6} \text{ s}^{-1}$ . Over the first 1200 s the relative concentration of **1b** diminishes relative to the shortest time interval of 480 s due to equilibration with **1c**. However, the two species are not at equilibrium at this point, and the average rate of appearance of **1a** lies between both values at  $4.9 \times 10^{-6} \text{ s}^{-1}$ . These observations are attributed to the fact that only one of **1b** and **1c** converts to **1a**. From these data, unstable **1b** is identified as the starting point of the pathway to stable **1a** (Figure 6).

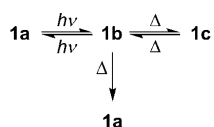


Figure 6. Representation of the observed photochemical/thermal equilibrium of **1**.

X-ray crystallographic analysis of **1a** showed that the axial orientation of the methyl group and the overall *anti*-folded geometry are key elements in this structure (Figure 7, left). The length of the central double bond (1.343 Å) is typical for an alkene, and the Newman projection viewed along the central double bond reveals that it is not as twisted as would be expected for an overcrowded alkene (torsion angles: C14–C15–C16–C17 =  $1.1(3)^\circ$  and C1–C15–C16–C28 =  $2.7(3)^\circ$ ; Figure 7, right). This is due to the flexibility introduced by the thiopyran and suberene subunits: the (least square) planes C26–S–C27 and C6–C7–C8–C9 are almost parallel (difference between the planes =  $11.6(1)^\circ$ ), which allows for relief of the steric strain.

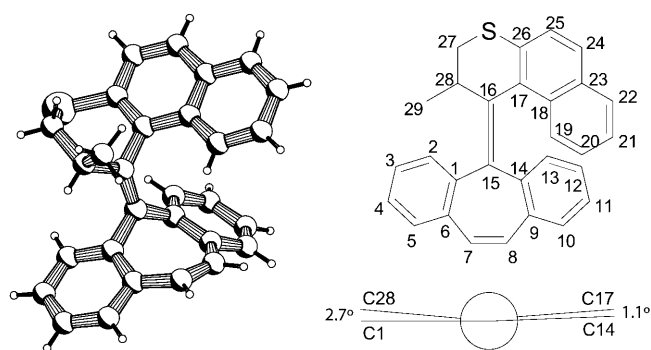


Figure 7. PLUTO plot of the X-ray structure of **1a** (left) and the Newman projection along the central double bond and numbering scheme adopted (right).

DFT calculations were performed by using the Gaussian 03 program package<sup>[18]</sup> to support the assignment of relative stabilities of the different conformers. In its lowest

energy conformation, compound **1** adopts an *anti*-folded geometry, with the methyl substituent at the stereogenic centre in an axial orientation (Figure 8a, **1a**). A higher energy conformation was identified as being *syn*-folded, with the methyl group adopting an axial orientation (**1b** in Figure 8a). It has a calculated energy of  $14.1 \text{ kJ mol}^{-1}$  relative to **1a**. This structure is formally a twisted structure, although it releases much of the strain by folding. A second local minimum was identified as having an *anti*-folded geometry, with the methyl group adopting an equatorial orientation (**1c** in Figure 8a). Structure **1c** is higher in energy than **1b** by  $1.4 \text{ kJ mol}^{-1}$ .

Calculations on the transition state reached during the isomerisation between **1b** and **1c** indicate that this process has a lower barrier than that for the isomerisation of **1b** to **1a**. The transition state **1(TS1)** for the interconversion of **1b** and **1c** (Figure 8a) was determined to involve an upper half ring flip during which the naphthalene part of the molecule passes the lower half, and was calculated to have an energy of  $97.8 \text{ kJ mol}^{-1}$  relative to the lower energy isomer **1b**. On the other hand, conversion of **1b** → **1a** was found to proceed through transition state **1(TS2)** with a flat suberene ring that had an energy of  $105.4 \text{ kJ mol}^{-1}$  relative to **1b**. A schematic representation of the potential-energy profile can be seen in Figure 8b.

In previous work, a similar molecular motor in which the thiopyran unit was substituted for a dihydrophenanthrene unit<sup>[10]</sup> was described (**2** in Scheme 1). However additional stable conformations were not noted.<sup>[17]</sup>

Calculations on a second-generation molecular motor composed of a thioxanthylene stator unit connected to a thiopyran rotor unit (**3**, Scheme 1)<sup>[10]</sup> suggest that thermal helix inversion is in fact a two-step process (Figure 9). The photochemical product observed experimentally by <sup>1</sup>H NMR spectroscopy (equatorial orientation of the stereogenic methyl group, **3c**) is calculated to have a higher energy than the lowest energy conformational isomer by  $19.3 \text{ kJ mol}^{-1}$ . The first step in thermal helix inversion to revert to the most stable conformation proceeds via **3(TS1)**, in which the naphthalene unit of the rotor flips over the lower half through an upper half ring flip. This pathway has a high energy of activation and leads to a twisted local minimum on the potential-energy surface with overall *syn*-folded geometry (**3b**). In this conformation the strain of the formally twisted, *syn*-folded geometry is relieved partly by the high degree of folding. Intermediate **3b** was not observed experimentally due to the much lower activation energy of the second thermal process. This process involves a lower half ring-flip, in which the stereogenic methyl group (or more specifically, the proton on the methyl group that is closest to the stator) passes the stator. It is represented by **3(TS1)** and **3(TS2)**, can theoretically be inverted, but results in a higher activation energy for the rate-determining step, making this pathway improbable.

Examination of the conformations of compound **4** at the same level of theory indicates that conformation **4b** is un-

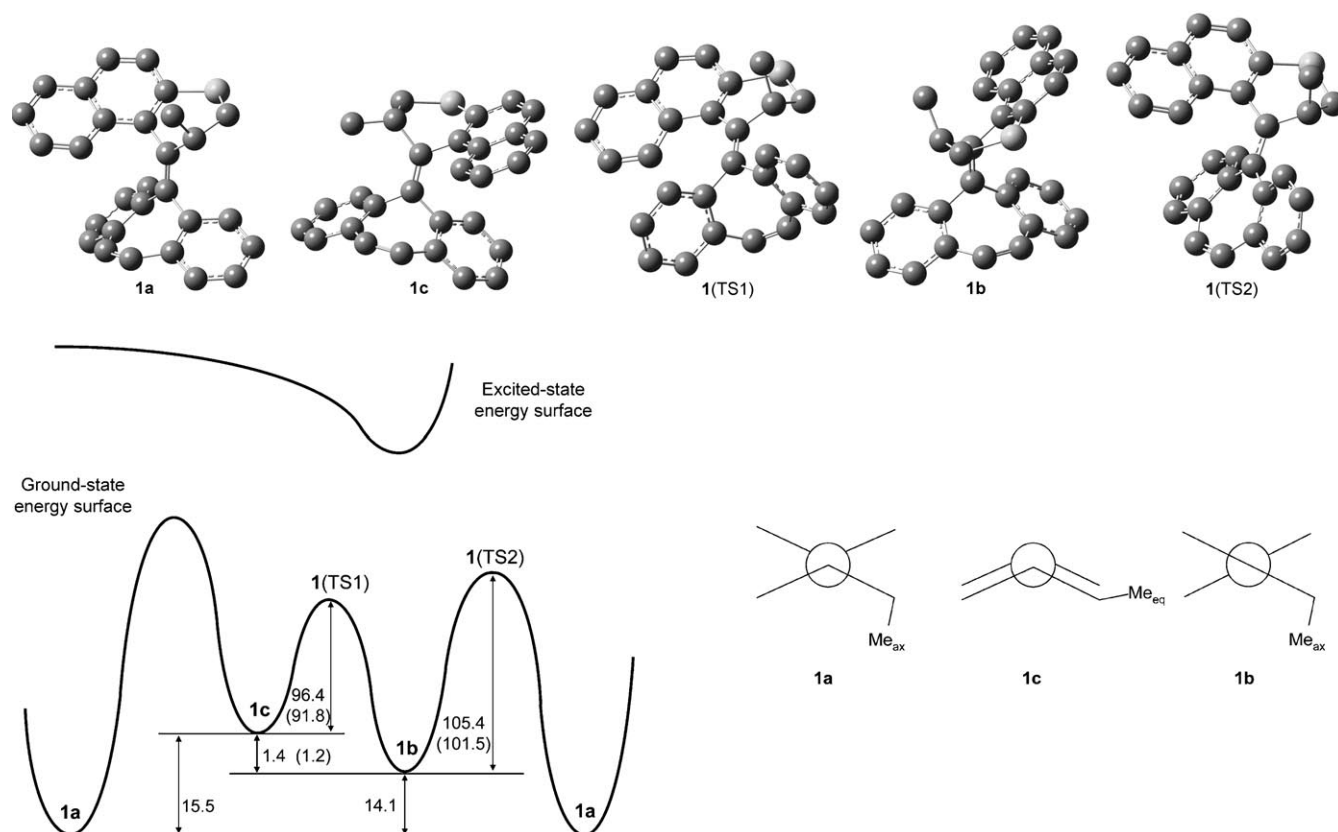


Figure 8. A) Conformations of second-generation motor **1** optimised by DFT calculations at the B3LYP 6-31G(d,p) level. From left to right: *anti*-folded Me<sub>ax</sub> (lowest energy) conformation **1a**, *anti*-folded Me<sub>eq</sub> conformation **1c** ( $E=15.5$  kJ mol<sup>-1</sup>), transition state **1(TS1)** for going from **1c** to **1b** ( $E=111.9$  kJ mol<sup>-1</sup>), *syn*-folded, formally twisted Me<sub>ax</sub> isomer **1b** ( $E=14.1$  kJ mol<sup>-1</sup>), transition state **1(TS2)** for going from **1b** to **1a** ( $E=119.5$  kJ mol<sup>-1</sup>). B) Schematic energy diagram of calculated energies [kJ mol<sup>-1</sup>] of conformations of **1** (experimental values in brackets). C) Schematic Newman projections of **1a-c**.

available with fluorenylidene stator units (Figure 10). This confirms earlier studies on related structures,<sup>[11]</sup> in which the higher energy isomer observed experimentally was found to have an equatorial orientation of the methyl group at the stereogenic centre and an overall twisted double bond. Due to the equatorial orientation of the methyl group, conformation **c** represents the closest experimentally observed conformation (Figure 10, **4c**). The difference is that in this case it adopts a twisted geometry to minimise steric strain because an overall *anti*-folding geometry similar to six- or seven-ring stators is not possible for a fluorenylidene stator. The only transition state in this pathway is **4(TS1)**, in which the naphthalene part passes the lower half by an upper half ring flip. Isomer **4c** is higher in energy by 19.4 kJ mol<sup>-1</sup> relative to **4a**, and **4(TS1)** has a calculated energy of 139.5 kJ mol<sup>-1</sup> relative to **4c**.

<sup>1</sup>H NMR spectroscopy verified the analysis of the isomerisation processes of compound **4**. Irradiation with 365 nm light resulted in conversion to a metastable isomer that reverted to the lowest energy conformation upon heating at 130 °C overnight. The most stable conformation was characterised as having the methyl group at the stereogenic centre in an axial orientation by the coupling constants of the ring protons ( $^3J(\text{H}^A, \text{H}^B)=7.4$  and  $^3J(\text{H}^A, \text{H}^C)=4.8$  Hz, compared

with Table 1). In the higher energy conformation, the methyl group adopted an equatorial orientation ( $^3J(\text{H}^A, \text{H}^B)=12.4$  and  $^3J(\text{H}^A, \text{H}^C)=3.9$  Hz, see Table 1 for comparison) and no other isomers were detected. Isosbestic points identified by UV/Vis spectroscopy suggest a single unimolecular process is observed (Figure 12). The photochemical equilibrium of **4** was located almost quantitatively to the side of the higher energy conformer, as determined by <sup>1</sup>H NMR spectroscopy (**4c/4a**=95:5). The rates of thermal helix inversion in the conversion of **4c**→**4a** were determined in the temperature range of 125–140 °C by UV/Vis spectroscopy, and standard Eyring plot analysis provided activation parameters for the process (Figure 13 and Table 3). Compound **5** displayed behaviour comparable with that of compound **4** in all respects.

The experimental data presented above support the following mechanism for thermal helix inversion of compound **1**: Photochemical *cis/trans* isomerisation of the most stable *anti*-folded conformation **1a** provides the *syn*-folded isomer **1b** with the stereogenic substituent remaining in an axial orientation (Scheme 2). The most stable conformation, **1a**, can be recovered from **1b** by a ring-flip of the lower half via **1(TS2)**. Furthermore, *syn*-folded isomer **1b** is in thermal equilibrium with *anti*-folded isomer **1c**, which has its stereo-

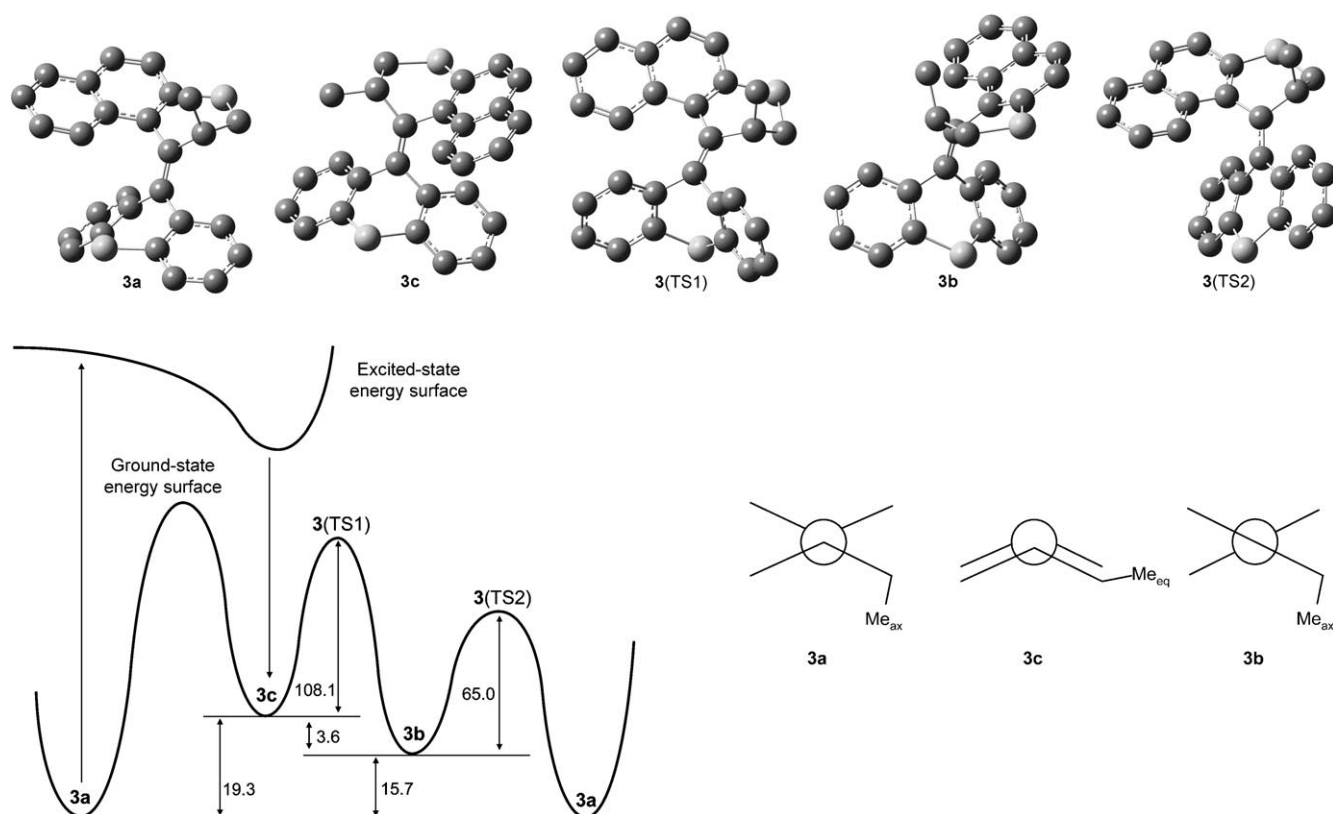


Figure 9. A) Conformations of second-generation motor **3** optimised by DFT calculations at the B3LYP 6-31G(d,p) level. From left to right: *anti*-folded Me<sub>ax</sub> (lowest energy) conformation **3a**, *anti*-folded Me<sub>eq</sub> conformation **3c** ( $E=19.3$  kJ mol<sup>-1</sup>), transition state **3(TS1)** for going from **3c** to **3b** ( $E=127.4$  kJ mol<sup>-1</sup>), *syn*-folded, formally twisted Me<sub>ax</sub> isomer **3b** ( $E=15.7$  kJ mol<sup>-1</sup>), transition state **3(TS2)** for going from **3b** to **3a** ( $E=80.7$  kJ mol<sup>-1</sup>). B) Calculated schematic energy levels [kJ mol<sup>-1</sup>] of different isomeric possibilities of molecular motor **3**. C) Schematic Newman projections of **3a–c**.

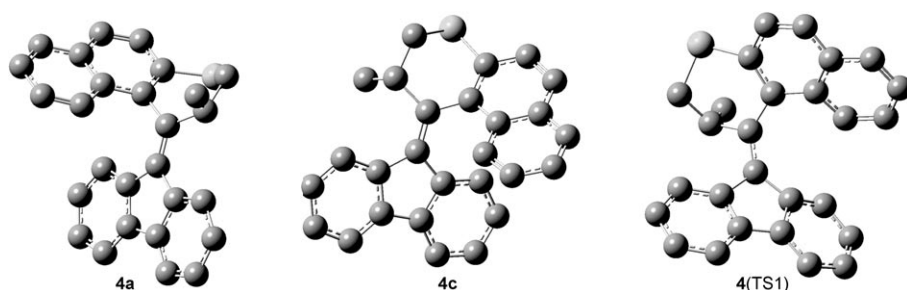


Figure 10. Conformations of second-generation motor **4** optimised with DFT calculations at the B3LYP 6-31G(d,p) level. From left to right: *anti*-folded Me<sub>ax</sub> (lowest energy) conformation **4a**, twisted Me<sub>eq</sub> conformation **4c** ( $E=19.4$  kJ mol<sup>-1</sup>) and transition state **4(TS1)** for going from **4c** to **4a** ( $E=158.9$  kJ mol<sup>-1</sup>).

genic substituent in an equatorial orientation, through an upper half ring flip involving **1(TS1)**. The availability of both conformers allows the motor to function by photochemical *cis/trans* isomerisation followed by lower half ring interconversion from *syn* to *anti*-folded. Therefore, the methyl group at the stereogenic centre is not required to adopt the more hindered equatorial orientation to complete a full half cycle, although it does so through the thermal equilibrium of **1b** with **1c**. This is in stark contrast with the mechanism reported for the second-generation molecular motors described previously. In all previous examples, the

outcome of the photochemical reaction involved a structure in which the stereogenic substituent was arranged in an equatorial orientation (conformation **c**). The main difference in the mechanism of thermal helix inversion of **1** compared to other molecular motors (including **2–5**) is therefore the initial photoproduct, which has its methyl group oriented in an axial orientation. With all conformations available for thio-

pyran upper half motors present in **1**, the different photochemical product allows us to study the mechanism experimentally in greater detail than has been possible thus far.

For the two thermally unstable isomers, the higher energy of *anti*-folded isomer **1c** than *syn*-folded isomer **1b** is in contrast to the results for dibenzocyclohepten-5-ylidene.<sup>[13]</sup> In the latter the *anti* conformer is lower in energy than the *syn*-folded conformer. This is in complete agreement with previous studies of molecular motors, in which the equatorial position of the stereogenic methyl group raises the energy with respect to axial orientation by steric repulsion with the

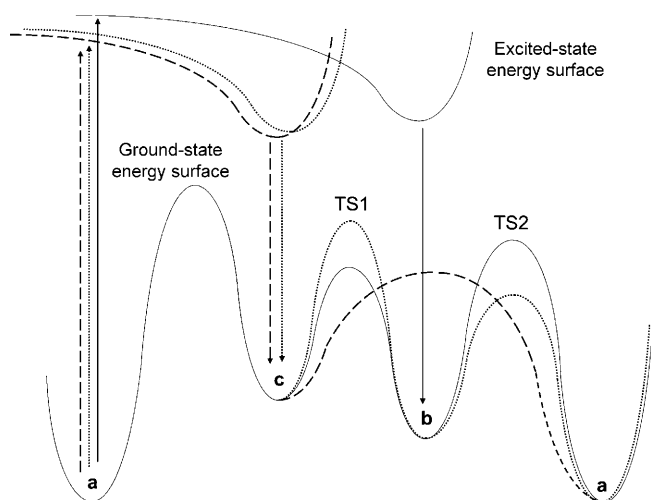


Figure 11. Comparison of the photochemistry and relative thermal stabilities for isomers of **1** (—), **3** (.....) and **4** (---).

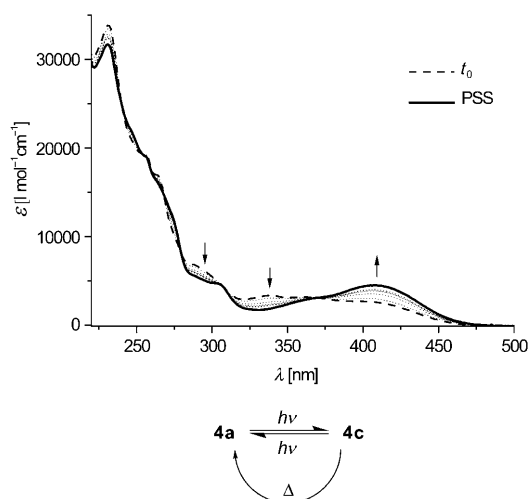


Figure 12. Top: UV/Vis spectra for the unimolecular photoisomerisation of **4**. Compound **5** displayed similar behaviour. Bottom: photochemical⇌thermal equilibrium of compound **4**.

stator unit. Therefore, calculated data are in full agreement with experimental observations and support the mechanism presented in Scheme 2.

With respect to **3**, in previous studies only one higher energy conformation has been observed experimentally, in which the stereogenic substituent is in an equatorial orientation. However, the calculations in the present report suggest that the thermal helix inversion is in fact a two-step process, with the same intermediates as observed for **1**. The difference in relative energies of the two transition states **3**(TS1) and **3**(TS2) preclude observation of the second conformation. Analysis of the representations of the minima and maxima on the potential-energy surface indicate that the overall conformations for **a**, **b**, **c**, TS1 and TS2 are the same in **1** and **3**. The most stable conformation, **a**, is described by an *anti*-folded geometry, with the methyl group at the stereogenic centre oriented in an axial orientation. Two higher

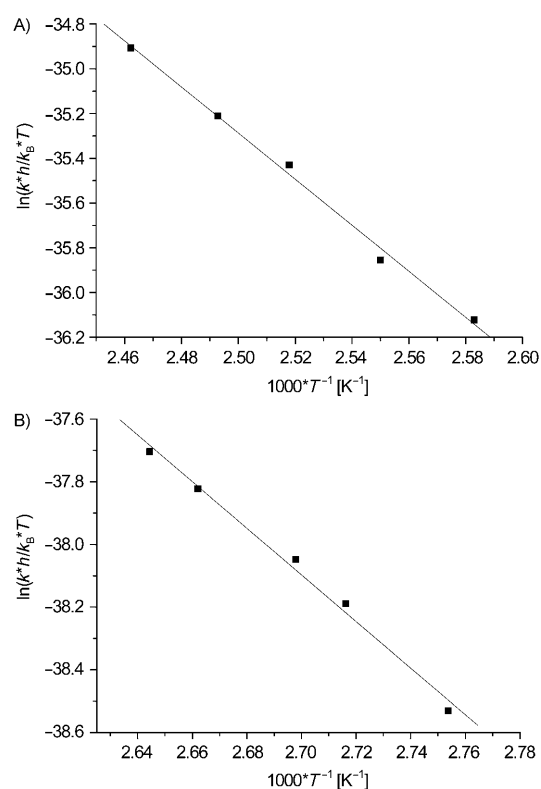
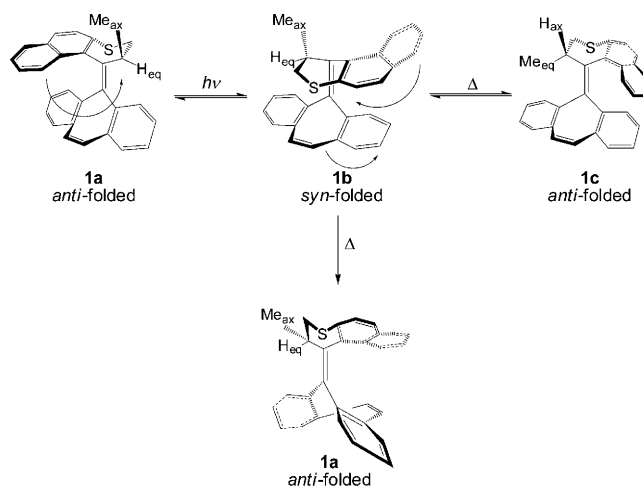


Figure 13. Eyring plots for A) thermal **4c**→**4a** conversion and B) thermal **5c**→**5a** conversion.

Table 3. Activation parameters for thermal helix inversion of motors **4** and **5**, and the extrapolated half-life at room temperature.

|          | $\Delta^\ddagger G^\circ$ [kJ mol <sup>-1</sup> ] | $\Delta^\ddagger H^\circ$ [kJ mol <sup>-1</sup> ] | $\Delta^\ddagger S^\circ$ [J K <sup>-1</sup> mol <sup>-1</sup> ] | $t_{1/2}$ [h] |
|----------|---|---|--|---------------|
| <b>4</b> | 109.0   | 85.6  | -79.4  | 829           |
| <b>5</b> | 105.8   | 61.9  | -149.7   | 226           |



Scheme 2. Proposed mechanism for one half rotation of molecular motor **1**.

energy conformations are distinguished, of which **c** is the highest in energy. It is represented by an overall *anti*-folded



geometry, with the methyl group at the stereogenic centre oriented in an equatorial orientation. This conformation is that described in our previous reports concerning the mechanism of thermal relaxation during rotation of second-generation molecular motors. However, during the process of thermal relaxation there is an additional minimum on the potential-energy profile, which had not been previously observed. This conformation, **b**, is characterised by a formally twisted, *syn*-folded geometry, with the methyl group at the stereogenic centre oriented in an axial orientation. This conformation, which can be observed experimentally only for **1**, is involved in the thermal relaxation to the lowest energy conformation **a**. The fact that we do not observe intermediate **b** in compound **2** indicates that, despite considerable similarities with the overcrowded di-5*H*-dibenzocyclohepten-5-ylidene, the observation of this conformation is not due solely to the presence of this stator unit. Rather, an intricate steric interplay between the 5*H*-dibenzocyclohepten-5-ylidene stator unit and the thiopyran rotor unit is proposed to be responsible for the observation of **1b**.

For **4**, only one high-energy conformation is observed. This can be attributed to the inability of the stator unit to adopt low-energy folding conformations. For this reason, the higher energy conformation comprises a twisted geometry with the methyl group at the stereogenic centre oriented in an equatorial orientation (conformation **4c**). One transition state involving an upper half ring flip (**4(TS1)**) connects **4c** to the most stable conformation **4a**.

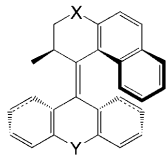
Based on the experimental results and calculations shown above, a general pattern for the higher energy structure in the rotation process of second-generation, light-driven molecular motors with thiopyran upper halves can be proposed. Motors with five-, six- and seven-ring stator units connected to a six-ring thiopyran rotor unit can be distinguished. A five-ring (fluorenylidene) stator unit reduces the flexibility of the structure overall, making isomer **b** inaccessible. The photochemical product is defined by the twisted conformation, **c**, which can regain the lowest energy conformation **a** through one transition state, involving an upper half ring flip. Stators with a central six- (**3**) or seven-ring (**1**) have one higher degree of conformational freedom, which results in two higher energy isomers, only one of which, normally, is observed experimentally. *Syn*- and *anti*-folded conformations can be distinguished; the *anti*-folded orientation is higher in energy due to an equatorial orientation of the stereogenic substituent.

However, the actual mechanism of rotation for these structures varies with the initial photochemical product after *cis/trans* isomerisation. For the central six-ring (thioxanthene) stator (**3**), the photochemical product has the overall *anti*-folded conformation with an equatorial orientation of the methyl group (**3c**). For a central unsaturated seven-ring (suberene) stator (**1**), the photochemical product is represented by the overall *syn*-folded conformation, with the methyl group at the stereogenic centre in an axial orientation (**1b**). The positions of the photochemical equilibria differ considerably however. This is possibly due to high

energy differences between the minima on the excited-state energy surface. For both structures, similar thermal pathways via similar transition states TS1 and TS2 are available. An important difference is the drastic change in energy of the transition states that govern the thermal conversion back to the most stable conformation, **a** (Figure 11), which results, in most cases, in only a single isomer being experimentally observed.

Re-analysing the activation parameters obtained for other structures, it can be seen that, in contrast to the literature,<sup>[16]</sup> the influence of the C–Y bond length on the isomerisation barrier of molecular motors is less clear. The C–Y–C distance is a major factor in determining the amount of steric hindrance in the fjord region, which is perceived to be an important factor in controlling the rate of the rate-determining step for thermal helix inversion. This effect is partly negated by conformational flexibility (Table 4). The rate of

Table 4. Gibbs energy of activation ( $\Delta^\ddagger G^\ominus$ ) for second-generation molecular motors [ $\text{kJ mol}^{-1}$ ] related to the distance ( $d$ ) between the carbon atoms connected to the central bridging atoms X and Y.



| X               | Y       | S    | CMe <sub>2</sub> | O                   | suberene | fluorene            |
|-----------------|---------|------|------------------|---------------------|----------|---------------------|
|                 | $d$ [Å] | 2.64 | 2.46             | 2.33                | 3.0      | 1.46                |
| CH <sub>2</sub> | 2.48    | 92   | 94               | n.d. <sup>[a]</sup> | 103      | 129 <sup>[19]</sup> |
| S               | 2.75    | 106  | 106              | 100                 | 101      | 109                 |

[a] n.d. = not determined.

thermal helix inversion is seen to increase when changing from fluorene to suberene to xanthene, with the rates for dimethylantracene and thioxanthene being comparable. The relatively low barriers associated with a central ring flip with these stator units are at the origin of this phenomenon. Higher barriers are associated with inflexible stator units, in particular the fluorenyl moiety.

## Conclusion

A new mechanism for thermal helix inversion has been identified for a dibenzocyclohepten-5-ylidene molecular motor. The transition state for interconversion of both higher energy isomers is lower than other comparable structures. Furthermore, the transition state for a lower-half ring flip is higher than related compounds. This allows, for the first time, experimental observation of both the *syn*- and the *anti*-folded conformations of the molecular motors. During the rotation cycle, the stereogenic substituent of this new motor is never required to adopt a more hindered equatorial orientation in contrast to all examples reported previously, although it does so through a second thermal isomerisation pathway.

This mechanism allows for a generalisation of the mechanistic pathway available for molecular motors. One stable and two higher energy conformations can be distinguished, with similar pathways connecting them. Fluorenylidene stators are different because these can only attain one higher energy, "twisted" conformation. Photochemical *cis/trans* isomerisation results in one of the higher energy structures, after which thermal pathways govern conversion to the lowest energy conformation. The conformational flexibility of the lower half is more important for the rate of thermal helix inversion than the C–Y–C bond length, which is due to extra flexibility in the transition state.

## Experimental Section

**General:**  $^1\text{H}$  NMR spectroscopic measurements were performed on a Varian Unity Plus spectrometer operating at 500 MHz and relative amounts of isomers were calculated by integration. Irradiation was performed in  $[\text{D}_6]$ toluene (reference Me at  $\delta = 2.09$  ppm) by using a Spectroline ENB-280C/FE UV lamp at 312 or 365 nm at room temperature or by using a cryostatic bath as required. UV/Vis spectra were measured on a Hewlett-Packard HP 8543 FT spectrophotometer equipped with a Quantum Northwest Peltier-cooled temperature controller for temperatures below 100 °C, with appropriate bandpass or cut-off filters in the beam to minimise photochemistry during measurement. For the high-temperature (>100 °C) measurements, a Jasco V-630 spectrophotometer equipped with a home-built cell holder connected to an ethylene glycol thermostatic bath was used. Calculations were carried out by using the Gaussian 03 program package using the density functional hybrid theory system (B3LYP).<sup>[18]</sup> Geometry optimisations were performed using the 6-31G(d,p) basis set, and were followed by frequency calculations to confirm that real maxima or minima on the energy surface had been reached. Single-point energies on optimised structures were performed by using a 6-311+G(2d,p) basis set. Intrinsic reaction coordinate (IRC) calculations were performed to verify that no minima had been omitted from consideration.

**Synthesis and characterisation:** The compounds not previously reported were prepared following procedures reported earlier for related molecular motors.<sup>[10,11]</sup>

**Compound 1:**<sup>[10]</sup>  $^1\text{H}$  NMR (400 MHz,  $\text{CD}_2\text{Cl}_2$ , 20 °C):  $\delta = 7.64$ – $7.35$  (m, 8H), 7.24–7.07 (m, 5H), 6.80 (dt,  $J = 7.5$ , 1.5 Hz, 1H), 6.64 (dt,  $J = 7.5$ , 1.5 Hz, 1H), 6.50 (d,  $J = 8.1$  Hz, 1H), 3.78 (m, 1H), 3.54 (dd,  $J = 11.7$ , 8.1 Hz, 1H), 2.79 (dd,  $J = 11.7$ , 4.8 Hz, 1H), 0.70 ppm (d,  $J = 7.0$  Hz, 3H);  $^{13}\text{C}$  NMR ( $\text{CD}_2\text{Cl}_2$ , 400 MHz, 20 °C):  $\delta = 141.4$  (C), 138.2 (C), 138.0 (C), 137.2 (C), 136.2 (C), 135.7 (C), 134.7 (C), 133.6 (C), 132.2 (CH), 131.8 (C), 131.6 (CH), 131.5 (C), 128.6 (CH), 128.5 (CH), 128.44 (CH), 128.40 (CH), 128.2 (CH), 127.7 (CH), 127.5 (CH), 127.2 (CH), 127.1 (CH), 126.4 (CH), 126.2 (CH), 125.9 (CH), 125.5 (CH), 124.8 (CH), 37.9 (CH<sub>2</sub>), 34.5 (CH), 19.9 ppm (CH<sub>3</sub>); EIMS:  $m/z$  (%): 402 (100), 387 (12), 185 (13); HRMS (EI):  $m/z$ : calcd for  $\text{C}_{20}\text{H}_{22}\text{S}$ : 402.1442; found: 402.1453.

**Compound 4:**<sup>[11]</sup>  $^1\text{H}$  NMR (400 MHz,  $\text{CDCl}_3$ , 20 °C):  $\delta = 8.08$  (dd,  $J = 6.2$ , 2.6 Hz, 1H), 7.61–7.57 (m, 2H), 7.87–7.83 (m, 3H), 7.79 (dd,  $J = 6.2$ , 1.5 Hz, 1H), 7.43–7.40 (m, 2H), 7.36 (dt,  $J = 6.6$ , 1.1 Hz, 1H), 7.22 (dt,  $J = 7.0$ , 1.5 Hz, 1H), 7.30 (dt,  $J = 7.3$ , 0.7 Hz, 1H), 6.53 (dt,  $J = 8.4$ , 1.1 Hz, 1H), 5.70 (d,  $J = 8.0$  Hz, 1H), 4.73–4.81 (m, 1H), 3.36 (dd,  $J = 12.1$ , 7.3 Hz, 1H), 2.60 (dd,  $J = 12.4$ , 7.7 Hz, 1H), 1.39 ppm (d,  $J = 7.0$  Hz, 3H);  $^{13}\text{C}$  NMR (400 MHz,  $\text{CDCl}_3$ , 20 °C):  $\delta = 142.1$  (C), 141.3 (C), 139.7 (C), 137.8 (C), 137.6 (C), 136.8 (C), 134.2 (C), 133.3 (C), 132.1 (C), 128.3 (CH), 128.2 (CH), 127.8 (CH), 127.3 (CH), 127.2 (CH), 127.1 (CH), 127.0 (CH), 126.7 (CH), 125.4 (CH), 125.2 (CH), 125.0 (CH), 124.6 (CH), 119.8 (CH), 118.8 (CH), 39.0 (CH<sub>2</sub>), 37.3 (CH), 18.6 ppm (CH<sub>3</sub>), one (C) signal was not observed; EIMS:  $m/z$  (%): 376 (100), 334 (87.5), 198 (24.8); HRMS (EI):  $m/z$ : calcd for  $\text{C}_{27}\text{H}_{20}\text{S}$ : 376.1271; found: 376.1286.

**Compound 5:**<sup>[11]</sup>  $^1\text{H}$  NMR (200 MHz,  $\text{CDCl}_3$ , 20 °C):  $\delta = 8.01$ – $7.91$  (m, 1H), 7.90–7.75 (m, 4H), 7.70 (d,  $J = 7.6$  Hz, 1H), 7.45–7.33 (m, 2H), 7.28 (dt,  $J = 7.4$ , 0.9 Hz, 1H), 7.10–7.20 (m, 3H), 6.72 (dt,  $J = 7.6$ , 0.7 Hz, 1H), 6.53 (d,  $J = 8.0$  Hz, 1H), 4.43 (m, 2H), 4.22 (m, 1H), 1.45 ppm (d,  $J = 7.0$  Hz, 3H);  $^{13}\text{C}$  NMR (500 MHz,  $\text{CDCl}_3$ , 20 °C):  $\delta = 153.4$  (C), 140.6 (C), 139.5 (C), 138.3 (C), 137.9 (C,C), 132.6 (C), 131.9 (C), 131.8 (CH), 129.0 (C), 128.3 (CH), 127.3 (CH), 127.1 (CH), 127.0 (CH), 126.8 (CH), 126.5 (CH), 125.2 (CH), 125.0 (CH), 124.4 (CH), 123.5 (CH), 119.9 (CH), 118.9 (CH), 118.1 (CH), 113.7 (C), 72.3 (CH<sub>2</sub>), 33.0 (CH), 15.8 ppm (CH<sub>3</sub>); HRMS (EI):  $m/z$ : calcd for  $\text{C}_{27}\text{H}_{20}\text{O}$ : 360.1514; found: 360.1503.

## Acknowledgements

The authors thank NanoNed and the Netherlands Organization for Scientific Research (NWO-CW) for financial support. We are grateful to Dr. Wesley Browne for valuable suggestions on the manuscript.

- [1] a) P. D. Boyer, *Angew. Chem.* **1998**, *110*, 2424; *Angew. Chem. Int. Ed.* **1998**, *37*, 2296; b) J. E. Walker, *Angew. Chem.* **1998**, *110*, 2438; *Angew. Chem. Int. Ed.* **1998**, *37*, 2308.
- [2] R. D. Vale, R. A. Milligan, *Science* **2000**, *288*, 88.
- [3] a) *Molecular Motors* (Ed.: M. Schliwa), Wiley-VCH, Weinheim, **2003**; b) G. S. Kottas, L. I. Clarke, D. Horinek, J. Michl, *Chem. Rev.* **2005**, *105*, 1281–1376; c) E. R. Kay, D. A. Leigh, F. Zerbetto, *Angew. Chem.* **2007**, *119*, 72–196; *Angew. Chem. Int. Ed.* **2007**, *46*, 72–191; d) W. R. Browne, B. L. Feringa, *Nat. Nanotechnol.* **2006**, *1*, 25; e) B. L. Feringa, *J. Org. Chem.* **2007**, *72*, 6635–6652; f) B. L. Feringa, R. A. van Delden, N. Koumura, E. G. Geertsema, *Chem. Rev.* **2000**, *100*, 1789–1816.
- [4] a) *Molecular Rotaxanes, Catenanes and Knots* (Eds.: J.-P. Sauvage, C. Dietrich-Buchecker), Wiley-VCH, Weinheim, **1999**; b) V. Balzani, M. Gómez-López, J. F. Stoddard, *Acc. Chem. Res.* **1998**, *31*, 405; c) for a special issue on molecular machines, see: *Acc. Chem. Res.* **2000**, *100*, 409.
- [5] a) C. M. Keaveney, D. A. Leigh, *Angew. Chem.* **2004**, *116*, 1242; *Angew. Chem. Int. Ed.* **2004**, *43*, 1222; b) D. W. Steuerman, H.-R. Tseng, A. J. Peters, A. H. Flood, J. O. Jeppesen, K. A. Nielsen, J. F. Stoddard, J. R. Heath, *Angew. Chem.* **2004**, *116*, 6648; *Angew. Chem. Int. Ed.* **2004**, *43*, 6486.
- [6] a) M. C. Jimenez, C. Dietrich-Buchecker, J.-P. Sauvage, *Angew. Chem.* **2000**, *112*, 3422–3425; *Angew. Chem. Int. Ed.* **2000**, *39*, 3284–3287; b) Y. Liu, A. H. Flood, P. A. Bonvallet, S. A. Vignon, B. H. Northrop, H.-R. Tseng, J. O. Jeppesen, T. J. Huang, B. Brough, M. Baller, S. Magonov, S. D. Solares, W. A. Goddard, C.-M. Ho, J. F. Stoddard, *J. Am. Chem. Soc.* **2005**, *127*, 9745–9759.
- [7] a) T. R. Kelly, H. De Silva, R. A. Silva, *Nature* **1999**, *401*, 150; b) T. R. Kelly, R. A. Silva, H. De Silva, S. Jasmin, Y. J. Zhao, *J. Am. Chem. Soc.* **2000**, *122*, 6935.
- [8] a) B. L. Feringa, *Acc. Chem. Res.* **2001**, *34*, 504; b) D. A. Leigh, J. K. Y. Wong, F. Dehez, F. Zerbetto, *Nature* **2003**, *424*, 174; c) S. P. Fletcher, F. Dumur, M. M. Pollard, B. L. Feringa, *Science* **2005**, *310*, 80; d) M. M. Pollard, M. Klok, D. Pijper, B. L. Feringa, *Adv. Funct. Mater.* **2007**, *17*, 718.
- [9] N. Koumura, R. J. W. Zijlstra, R. A. van Delden, A. Meetsma, *Nature* **1999**, *401*, 152.
- [10] N. Koumura, E. M. Geertsema, M. B. van Gelder, A. Meetsma, B. L. Feringa, *J. Am. Chem. Soc.* **2002**, *124*, 5037.
- [11] a) J. Vicario, M. Walko, A. Meetsma, B. L. Feringa, *J. Am. Chem. Soc.* **2006**, *128*, 5127; b) J. Vicario, A. Meetsma, B. L. Feringa, *Chem. Commun.* **2005**, 5910.
- [12] M. K. J. Ter Wiel, R. A. van Delden, A. Meetsma, B. L. Feringa, *J. Am. Chem. Soc.* **2005**, *127*, 14208.
- [13] a) P. U. Biedermann, J. J. Stezowski, I. Agranat, *Eur. J. Org. Chem.* **2001**, *15*; b) W. R. Browne, M. M. Pollard, B. de Lange, A. Meetsma, B. L. Feringa, *J. Am. Chem. Soc.* **2006**, *128*, 12412.

- [14] A. Schönberg, U. Sadtke, K. Präfcke, *Chem. Ber.* **1969**, *102*, 1453.
- [15] a) N. A. Bailey, S. E. Hull, *Acta Crystallogr. Sect. B* **1978**, *34*, 3289;  
b) J.-S. Lee, S. C. Nyburg, *Acta Crystallogr. Sect. C* **1985**, *41*, 560;  
c) P. U. Biedermann, A. Levy, M. R. Suissa, J. J. Stezowski, I. Agrinat, *Enantiomer* **1996**, *1*, 75.
- [16] B. L. Feringa, W. F. Jager, B. de Lange, *Tetrahedron Lett.* **1992**, *33*, 2887.
- [17] A re-examination of this structure in the temperature range of  $-50$  to  $+60$  °C in the context of the current study does not affect the validity of conclusions presented earlier.
- [18] Gaussian 03, Revision C.02, M. J. Frisch, G. W. Trucks, H. B. Schlegel, G. E. Scuseria, M. A. Robb, J. R. Cheeseman, J. A. Montgomery, Jr., T. Vreven, K. N. Kudin, J. C. Burant, J. M. Millam, S. S. Iyengar, J. Tomasi, V. Barone, B. Mennucci, M. Cossi, G. Scalmani, N. Rega, G. A. Petersson, H. Nakatsuji, M. Hada, M. Ehara, K. Toyota, R. Fukuda, J. Hasegawa, M. Ishida, T. Nakajima, Y. Honda, O. Kitao, H. Nakai, M. Klene, X. Li, J. E. Knox, H. P. Hratchian, J. B. Cross, C. Adamo, J. Jaramillo, R. Gomperts, R. E. Stratmann, O. Yazyev, A. J. Austin, R. Cammi, C. Pomelli, J. W. Ochterski, P. Y. Ayala, K. Morokuma, G. A. Voth, P. Salvador, J. J. Dannenberg, V. G. Zakrzewski, S. Dapprich, A. D. Daniels, M. C. Strain, O. Farkas, D. K. Malick, A. D. Rabuck, K. Raghavachari, J. B. Foresman, J. V. Ortiz, Q. Cui, A. G. Baboul, S. Clifford, J. Cioslowski, B. B. Stefanov, G. Liu, A. Liashenko, P. Piskorz, I. Komaromi, R. L. Martin, D. J. Fox, T. Keith, M. A. Al-Laham, C. Y. Peng, A. Nanayakkara, M. Challacombe, P. M. W. Gill, B. Johnson, W. Chen, M. W. Wong, C. Gonzalez, J. A. Pople, Gaussian, Inc., Wallingford CT, **2004**.
- [19] In contrast with that previously reported in ref. [11b].

Received: May 21, 2008

Revised: July 28, 2008

Published online: October 31, 2008